






Review

# A Review of the Impact of Zinc Oxide Nanostructure Morphology on Perovskite Solar Cell Performance

Matshidiso Manabeng <sup>1,\*</sup> , Bernard S. Mwankemwa <sup>2</sup> , Richard O. Ocaya <sup>3</sup> , Tshwafo E. Motaung <sup>4,5</sup>  and Thembinkosi D. Malevu <sup>1,\*</sup> 

- <sup>1</sup> Department of Physics, Sefako Makgatho Health Sciences University, P.O. Box 94, Medunsa 0204, South Africa  
<sup>2</sup> Energy and Materials Research Laboratory, Department of Physics, College of Natural and Mathematical Sciences, University of Dodoma, P.O. Box 338, Dodoma 41218, Tanzania  
<sup>3</sup> Department of Physics, University of the Free State, P. Bag X13, Phuthaditjhaba 9866, South Africa  
<sup>4</sup> Department of Chemistry, School of Science in the College of Science Engineering and Technology, University of South Africa, UNISA, P.O. Box 392, Pretoria 0003, South Africa  
<sup>5</sup> Department of Chemistry, Sefako Makgatho Health Sciences University, P.O. Box 235, Medunsa 0204, South Africa  
\* Correspondence: 201609508@swave.smu.ac.za (M.M.); thembinkosi.malevu@smu.ac.za (T.D.M.)

**Abstract:** Zinc oxide (ZnO) has been widely studied over the last decade for its remarkable properties in optoelectronic and photovoltaic devices because of its high electron mobility and excitonic properties. It has probably the broadest range of nanostructured forms that are also easy and cheap to synthesize using a wide variety of methods. The volume of recent work on ZnO nanostructures and their devices can potentially overshadow significant developments in the field. Therefore, there is a need for a concise description of the most recent advances in the field. In this review, we focus on the effect of ZnO nanostructure morphologies on the performance of ZnO-based solar cells sensitized using methylammonium lead iodide perovskite. We present an exhaustive discussion of the synthesis routes for different morphologies of the ZnO nanostructure, ways of controlling the morphology, and the impact of morphology on the photoconversion efficiency of a given perovskite solar cell (PSC). We find that although the ZnO nanostructures are empirically similar, one-dimensional structures appear to offer the most promise to increasing photoconversion efficiency (PCE) by their proclivity to align and form vertically stacked layers. This is thought to favor electron hopping, charge mobility, and conductivity by allowing multiple charge conduction pathways and increasing the effective junction cross-sectional area. The combined effect is a net increase in PCE due to the reduced surface reflection, and improved light absorption.

**Keywords:** ZnO morphologies; perovskite; efficiency; photovoltaic devices



**Citation:** Manabeng, M.; Mwankemwa, B.S.; Ocaya, R.O.; Motaung, T.E.; Malevu, T.D. A Review of the Impact of Zinc Oxide Nanostructure Morphology on Perovskite Solar Cell Performance. *Processes* **2022**, *10*, 1803. <https://doi.org/10.3390/pr10091803>

Academic Editors: Sheng Hsiung Chang and Fang-Chung Chen

Received: 1 August 2022

Accepted: 27 August 2022

Published: 7 September 2022

**Publisher's Note:** MDPI stays neutral with regard to jurisdictional claims in published maps and institutional affiliations.



**Copyright:** © 2022 by the authors. Licensee MDPI, Basel, Switzerland. This article is an open access article distributed under the terms and conditions of the Creative Commons Attribution (CC BY) license (<https://creativecommons.org/licenses/by/4.0/>).

## 1. Introduction

ZnO is a metal oxide semiconductor that has a wide band gap of 3.37 eV and a large exciton binding energy of 60 meV [1–8]. These properties allow it to interact efficiently in emissive processes that involve excitons [9]. There is great interest in ZnO because of its promising properties and wide range of applications. For instance, it has high infrared reflectivity and good visible-spectrum transparency, is biocompatible, and its nanostructures show the greatest variety and are easy to prepare. Its high electron mobility means that the mean diffusive-transfer speed of its photo-generated electrons is high, making it suitable for optoelectronic and photovoltaic devices [1,2,6,8,10]. Chemically, it is stable, inexpensive, and environmentally friendly. ZnO is suitable for solution-based processing at lower temperatures because it is nearly soluble in water [4]. It has the appearance of a white to yellowish-white crystalline material. ZnO comes in three crystallization forms: cubic zinc blende, hexagonal wurtzite, and cubic rock salt. The various crystal structures of ZnO are shown in Figure 1. The rocksalt structure is rare and only sporadically detected.

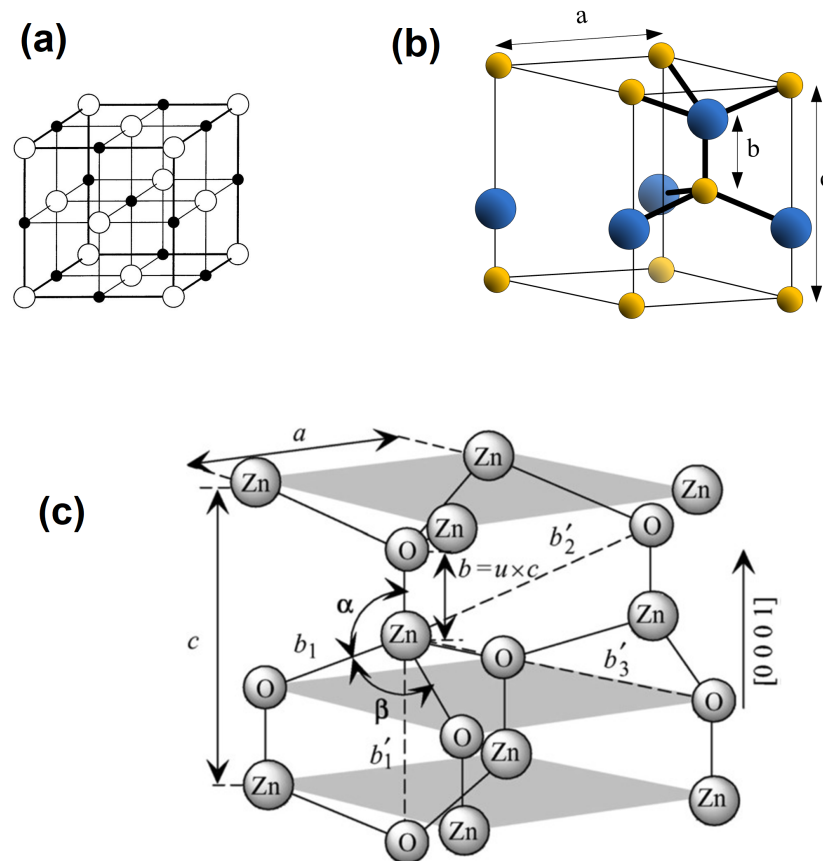


**Figure 1.** Structures of ZnO. In (a) cubic rocksalt, in (b) wurtzite hexagonal, and in (c) the wurtzite lattice constants  $a$  and  $c$ .

In contrast, the hexagonal wurtzite crystal structure shown in Figure 1a,b is stable at ambient temperature and pressure and more abundant. ZnO is a polar crystal with octahedral geometry. There are two lattice constants ( $a$  and  $c$ ) with hexagonal unit cells. It belongs to the space group  $C4_6v$  or  $P6_3mc$  [5]. The cubic martensite forms under high pressure conditions and is an indirect bandgap semiconductor ( $E_g = 2.7$  eV) [11]. The ZnO hexagonal lattice belongs to the space group of  $P6_3mc$  or  $C4_6v$ . It has lattice constants  $a = b = 0.32539$  nm and  $c = 0.52098$  nm such that  $c/a = \sqrt{8/3} = 1.6333$  [1,3,8,11,12]. The wurtzite structure consists of alternating planes of  $O^{2-}$  and  $Zn^{2+}$  ions coordinated to tetrahedra stacked along the  $c$ -axis. The base  $(0001)$  and  $(000\bar{1})$  planes have different bulk terminations, first with a positive Zn charge and second with a negative O charge. As a result of these polar surfaces, ZnO exhibits normal dipole moments and spontaneous polarization along the  $c$ -axis [13]. Normally, ZnO has three types of high-speed growth directions:  $(\pm[2\bar{1}\bar{1}0], \pm[\bar{1}2\bar{1}0], \pm[\bar{1}\bar{1}20])$ ,  $(\pm[01\bar{1}0], \pm[10\bar{1}0], \pm[1\bar{1}00])$  and  $\pm[0001]$  [12]. Since the energy of the  $(0001)$  crystal surface is higher than that of the other planes, as described above, the ZnO crystal tends to grow in the  $[0001]$  direction or along the  $c$ -axis. However, by adjusting the growth rate in these directions, a wide range of morphologies with major crystal facets can be obtained as shown in Figure 2. This highlights the vast variety of ZnO morphological structures, i.e., 1-dimension (1D), 2-dimension (2D), and 3-dimension (3D).

The 1D structures are the main and largest group and it includes nanorods, nanotubes, nanoneedles, nanohelices, nanorings, nanobelts, nanowires, and nanoneedles. The 2D structures have a greater surface area for dye-sensitized solar cells, including nanopellets, nanosheets, and nanoplates. The 3D structures include snowflakes, flowers, dandelions, and coniferous urchins [1–8,10–12]. Figure 3 shows various morphologies that can be seen under a scanning microscope. These forms are manifestations of the ZnO wurtzite structure possible from Figure 2.

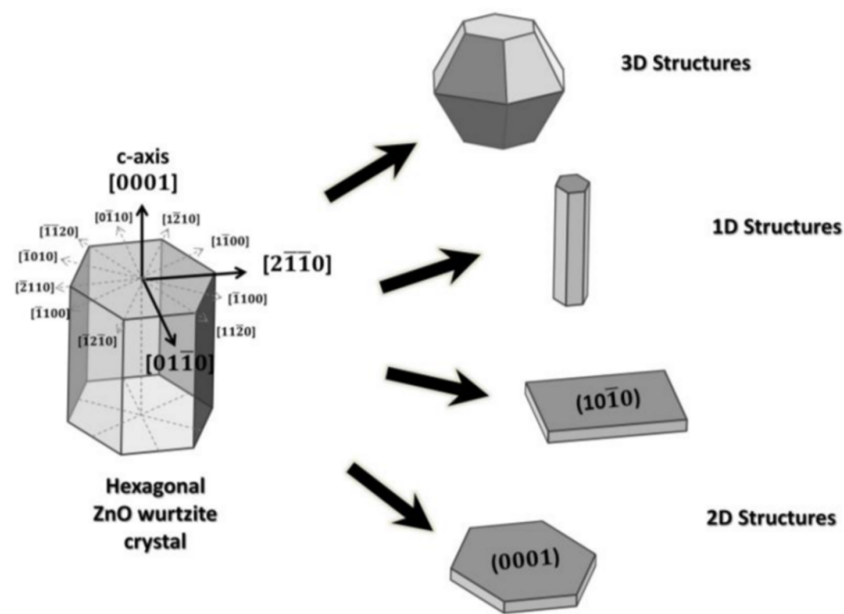


**Figure 2.** Preferential growth directions of ZnO wurtzite crystal and possible structures. Reproduced with permission from [14].

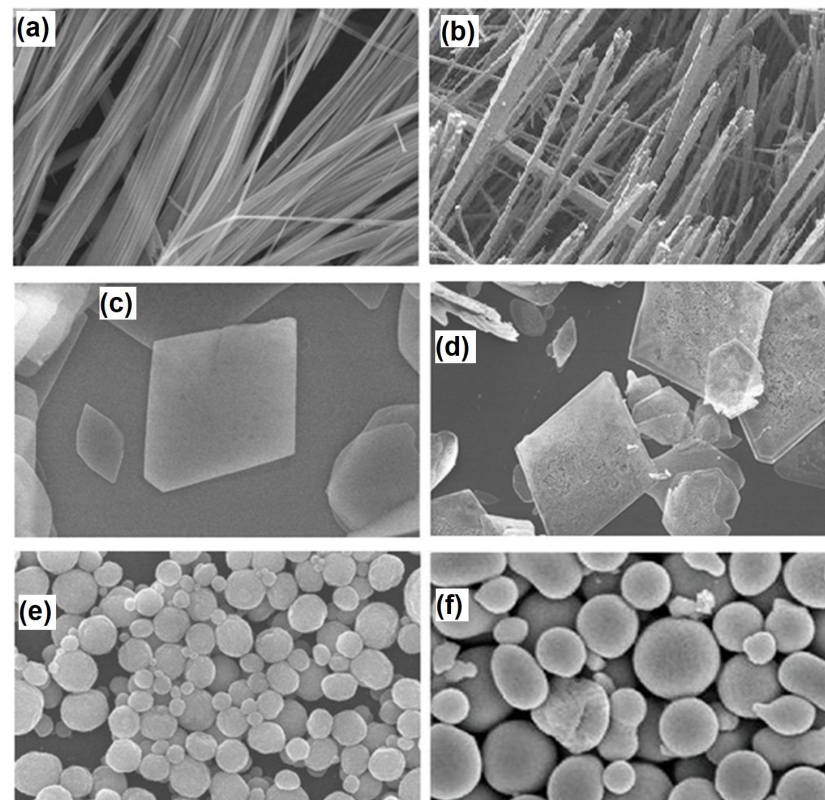


**Figure 3.** Typical examples of the morphologies of ZnO. (a,b) show 1D structures, (c,d) show 2D structures, while (e,f) show 3D structures. Reproduced with permission from [14].

#### *Application of ZnO Nanostructures in Perovskite Solar Cells*

Earlier in the search for the electron transporting materials certain oxides, particularly  $\text{SnO}_2$  and  $\text{TiO}_2$ , were shown to have some promising properties [15]. However, the research focus has largely shifted to ZnO-based materials. ZnO is physically similar [16,17] to both  $\text{SnO}_2$  and  $\text{TiO}_2$  but exhibits higher electron mobility and affinity. ZnO nanostructured materials appear to form a better electron transport layer than  $\text{SnO}_2$  and  $\text{TiO}_2$  [18]. In

addition, they can be manufactured using many simple methods and tuned by various synthesis conditions, such as precursor concentration [8], are less costly and use far less energy, and show greater robustness to detrimental environmental conditions such as photo-corrosion [19]. Several studies have established the influence of different hybrid configurations of ZnO nanoparticles on the application of the electron transport layer. The use of ZnO in third-generation solar cells has been widely reported in the literature. Such devices have employed ZnO in sensitizers in various configurations, most notably in dye-sensitized solar cells (DSSCs), quantum dots sensitized solar cells (QDSSCs), and perovskite-sensitized solar cells (PSSCs or PSCs). In DSSCs, the most common sensitizers are Phyto-dye extracts and derived complexes which, under monochromatic light, gave photo conversion efficiencies above 2% [20]. However, the role of ZnO was often limited under certain operating conditions when used jointly with other complexes in contrast to TiO<sub>2</sub>, which appeared to function more effectively due to its lower alkalinity. For example, ruthenium complexes were commonly used and appeared to improve the device performance, but the resulting acidity due to the protonation of the carboxyl groups of the Ru dye led to the dissolution of ZnO at the interfaces, with a replacement of Ru by Zn<sup>2+</sup> in the dye. The overall effect is that the chemical stability of ZnO is reduced. The net effect is that electron injection into the oxide is inhibited [21]. ZnO nanostructured materials have also been deployed as photoanodes in QDSSCs. One-dimensional structures, e.g., nanorods, nanotubes, and nanowires, appear to benefit from an increase in the photoconversion efficiencies owing to the natural vertical alignment of these structures, which is thought to favor electron hopping in stacked-layer devices such as solar cells. In addition, the surface defects are typically fewer, giving more charge conduction pathways and, therefore, lower device resistance and higher photocurrent in the material. However, they have been shown to be limited by their lower light harvesting abilities [22,23]. Perovskites, which quickly appeared on the scene as potential advancements, belong to materials with the ABX<sub>3</sub> structure. A and B are cations with different ionic radii, and X is an anion. Kojima et al. [24] first demonstrated that methyl ammonium lead halide perovskites appropriately sensitized TiO<sub>2</sub> under visible light. They reported PCE of 3.8% and 3.1% for the bromide and iodide perovskite versions, respectively [25]. The pace of research in PSCs has accelerated over the last decade, with PCEs of more than 20% now being reported routinely [24]. The strength of TiO<sub>2</sub> and ZnO in most of these devices is due to their inclination toward n-type, which enhances their ability to extract and transport photogenerated electrons, while simultaneously blocking photogenerated holes. Thus, the recombination of electron-hole pairs within the bulk is suppressed, leading to a higher photocurrent. It is, therefore, crucial to tailor the physical characteristics of the precursors of the device, i.e., the morphology, defects states, interfacial aspects, and energy alignment deployed to usher the final device into optimal performance [24,26]. It is now widely accepted that control of these parameters can be exerted gainfully through the synthesis and device fabrication method. Among the most impactful control pathways are the oxide nanostructure and interface engineering [16,18–20], the deposition method, post-treatment such as thermal decomposition [20], and doping [21–23,27–29]. The first reported application of ZnO as an electron transport layer (ETL) for PSCs was by Kumar et al. [30]. In their study, ZnO had the dual function as a hole-blocking compact layer and also as an electron-transporting layer with a mesoscopic nanorod structure. The compact layer was electrodeposited, and the nanorods were grown by chemical bath deposition. Planar devices using only compact ZnO layers have been demonstrated, albeit with lower J<sub>sc</sub> and FF than mixed compact/nanorod-based devices, with a conversion efficiency of 8.90% in contrast to ~2.62% that is typical for compact ZnO devices. Bi et al. [31] used an aligned array of ZnO nanorods as the ETL. Their results showed that ZnO nanorod-based PSCs exhibit good long-term stability, suggesting that perovskite materials are more suitable to sensitize ZnO nanorods. However, under AM 1.5G lighting, the efficiency of such solar cells is typically only 5.0%, due to the greater loss of recombination than for comparable TiO<sub>2</sub> devices. Such studies further evidence that the growth processes for ZnO nanorod

arrays, just as for the other structures, affect the performance of the final PSC. However, with ZnO, there are some limitations to its application in various devices, particularly PSCs [31–36].

Although there have been significant advances in recent years in ZnO-based PSCs, the literature suggests that many questions remain unanswered about the precise routes to apply ZnO nanoparticles in electronic devices and sensors. A quick online search returns thousands of articles pertaining to ZnO nanostructures in optoelectronic devices and suggesting possible directions. To this end, Table 1 summarizes recently reported PCE figures for ZnO-based PSCs.

**Table 1.** A brief summary of recent results on the impact of ZnO structure, synthesis method, post-treatment, and doping on the PCE of the PSC device.

Structure	Synthesis Method	Post-Treatment	Doping	PCE (%)
Nanorods	Spin coating	Polyethylene terephthalate capping Al <sub>2</sub> O <sub>3</sub> passivation	-	9.1 [34]
			-	10.0 [36]
			-	11.0 [1]
	Low-aspect ratio methods		-	10.3 [36]
			Nitrogen	11.6 [36]
	High-aspect ratio methods		Nitrogen	13.6 [36]
			Nitrogen	16.1 [1]
Hydrothermal	-	10.4 [19]		
	Magnesium	15.3 [37]		
	Iodine	18.2 [37]		
Nanoparticles	Non-aqueous method	Thermal decomposition	-	4.3 [38]
	Spin coating		-	7.0 [39]
	Spin coating (ZnO and ZnS blend)		-	10.9 [37]
	Spin coating		-	13.1 [8]
	Hydrothermal		Iodine	18.2 [37]
	RF magnetron sputtering		Gallium	20.2 [40]

The immense interest in ZnO nanostructures spanning more than a decade is evident in Table 1. Improvements in PCE have been possible by adjusting the morphology of ZnO nanoparticles, varying the synthesis method, post-treatment, and doping. It is probable that newer, improved approaches may still be found that further improve device PCE.

## 2. Synthesis Routes for ZnO Nanostructures

The synthesis method is now widely accepted as significantly influencing the final ZnO nanostructure, morphology, valence state, and defect distributions in the oxide lattice. The electrical, magnetic, mechanical, optical, and chemical properties can also be controlled through the synthesis method employed. The various nanostructure synthesis methods are broadly categorized into three groups, namely, chemical, physical, and green routes [41–44]. Chemical synthesis is the most widely used approach to synthesize ZnO nanostructures. This method can be classified as either the liquid or gaseous phase. Liquid-phase synthesis includes precipitation, co-precipitation method, colloidal methods, sol–gel processing, water–oil micro-emulsions method, hydrothermal synthesis, solvothermal, and sonochemical and polyol method [41,44–46]. However, gas-phase methods involve pyrolysis and inert gas condensation. Chemical synthesis, i.e., the bottom-up approach, combines substances in wet chemistry while adjusting reaction parameters. Atoms, molecules, or ions in the solution first nucleate, followed by cumulative aggregation of the species until the required nanosize regime is reached [46]. Physical synthesis, or the top-down approach, starts with the bulk matter and then breaks down the smaller particles until the nanoscale size is achieved. These methods include laser ablation, ball milling, melt mixing, physical vapor deposition, sputter deposition, electric arc deposition, and ion implantation. Green synthesis employs microorganisms or plant extracts with a precursor to form the

desired nanomaterials [46–48]. Table 2 summarizes the advantages and disadvantages of the chemical, physical, and green route synthesis methods.

**Table 2.** A summary of the various synthesis methods, and their advantages and disadvantages.

Method	Mode	Pros	Cons
Chemical	Hydrothermal, sol–gel, precipitation, co-precipitation, microwave, pyrolysis, micro-emulsion, thermal decomposition, bath deposition	Supports many precursors, and conditions. Allows tuning of morphology, size, and geometry	A large number of surfactants, poor solubility for some precursors, poor temperature stability of micro-emulsions, and pH issues [49]
Physical	Laser ablation, ball milling, melt mixing, physical vapor deposition, sputtering	Technically simple, chemically pure, uniform nanoparticles, applicable zinc surface	Needs higher energy, temperature and pressure, are expensive, and radiation fallout
Green	Plant extractions, biochemical, and microorganisms	Cost-effective, fewer toxic chemicals, use natural antimicrobe activity	Hard to tune size, shape, and growth rate. Endotoxin fallout, rarely reported in the literature

The growing body of literature shows that many synthesis modes have been developed for convenient and simple means of achieving the desired properties of these nanostructures. ZnO materials, a group II–VI binary compound semiconductors, have been considered in solar cell applications due to their stability, high conductivity, high electron affinity, and excellent electron mobility. Variations in ZnO nanostructures have a significant impact on three aspects of the solar cell film: (i) the solar layer morphology and loading, (ii) the quality of the ZnO/active layer interface, and (iii) as a conducting substrate as a photoanode. The ZnO nanomaterials grown directly on the substrate have been attractive due to their unique electron pathways, which suppress the influence of surface states typically found in the former case. This review presents and discusses recent progress on ZnO nanostructures, synthesis methods, and their effects on perovskite-sensitized solar cells. In this section, the focus is on the processes of synthesis and growth that are commonly used to realize the wide forms of ZnO nanoparticles. The influence of several parameters, such as pressure, temperature, pH, agitation, amount of reagent/substrate interface, presence of a catalyst, and concentration of the reagents during the course of the reaction, is discussed in this section.

### 2.1. Hydrothermal Synthesis of ZnO Nanostructures

With continued development and progress in material science, new powder synthesis and material preparation technologies are receiving increasing attention. The hydrothermal synthesis process is a promising liquid-phase technology that was developed in recent years. The microwave hydrothermal method makes good use of microwave-induced temperatures to compensate for the poor heating of the other hydrothermal methods, thus allowing practical application [48]. Hydrothermal synthesis refers to the heterogeneous reaction to synthesize inorganic materials in aqueous media above ambient temperature and pressure. In this case, the aqueous mixture of precursors is heated above the boiling point of water in a sealed stainless steel autoclave, resulting in a dramatic increase in pressure in the reaction autoclave above atmospheric pressure. This synergistic effect of high temperature and pressure provides a one-step process for producing highly crystalline materials without the need for post-annealing treatment. Hydrothermal strategies for synthesizing various nanomaterials, including ZnO nanomaterials, have also been developed. Reaction parameters such as precursor properties and concentrations, solvents, stabilizers, reaction temperature, and time have important effects on the product. Hydrothermal synthesis can yield very high crystallinity ZnO nanomaterials under high temperature and high pressure reaction conditions, compared to the “low temperature” co-precipitation method,

which usually produces low crystallinity nanoparticles. The hydrothermal approach yields relatively low product yields compared to the co-precipitation method. This method is commonly employed to synthesize well-aligned ZnO nanorods for the electron transport layer of solar cells. Figure 4 shows the schematic synthesis route for ZnO nanorods using water as the solvent. Typically, the method uses high autoclaving temperatures between 100–1000 °C and high pressures between 1–10,000 atmospheres.

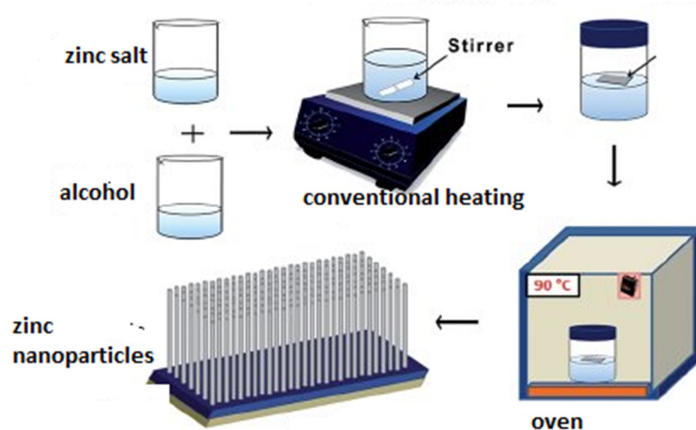


**Figure 4.** Overview of the hydrothermal method to synthesize ZnO nanoparticles. Reproduced with permission from [50].

Noorasid et al. [51] synthesized ZnO nanorods for use as an electron transport layer in a dye-sensitized solar cell using a hydrothermal method. In their study, they varied the time of the growth process to obtain a pristine layer of ZnO nanorods. The duration of the growth process was kept between 5 and 15 h, followed by annealing at 90 °C for 180 min. These variations in the synthesis conditions gave well vertically-aligned ZnO nanorods of uniform size and diameter. Similarly, Kumar et al. [52], while studying the effect of reaction time (3, 6, 9, and 12 h), obtained well-aligned ZnO nanorods with average lengths between 77 and 255 nm. Nadargi et al [53] demonstrated the flexibility of producing vertically aligned ZnO nanorods which are 700–800 nm long at lower hydrothermal temperature (80 °C) and shorter reaction time (2–10 h). It became evident that hydrothermal methods are more amenable to the control of synthesis parameters and thus permit the tuning of the properties of especially one-dimensional ZnO nanostructures. This approach is essential to optimize solar cell performance. The facile approach of the hydrothermal method proves effective in producing well-defined ZnO nanorods [54]. Figure 5 shows the overall SEM images of ZnO nanorods obtained under different conditions in the hydrothermal method.

Although hydrothermal synthesis has advantages over conventional synthesis, its reliance on high reaction temperatures and pressures and the longer reaction times are drawbacks, particularly for pilot and industrial-scale production. However, its allowance to tune the reaction temperature and reaction time makes it suitable for reaching the desired nanomaterial morphologies shown in Figure 5. Controlling the annealing temperature and reaction time can further enhance and improve the quality of the final nanorods by increasing their diameter and length [44]. The literature also has several accounts of hydrothermal synthesis in combination with other factors. For example, well-defined pencil-shaped ZnO nanorods have been reported in the method in the presence of surfactants [10]. Other structures reported are long ZnO nanowire arrays [3], nanobelts and nanospheres [54], nanoflowers [55], and nanotubes [56].

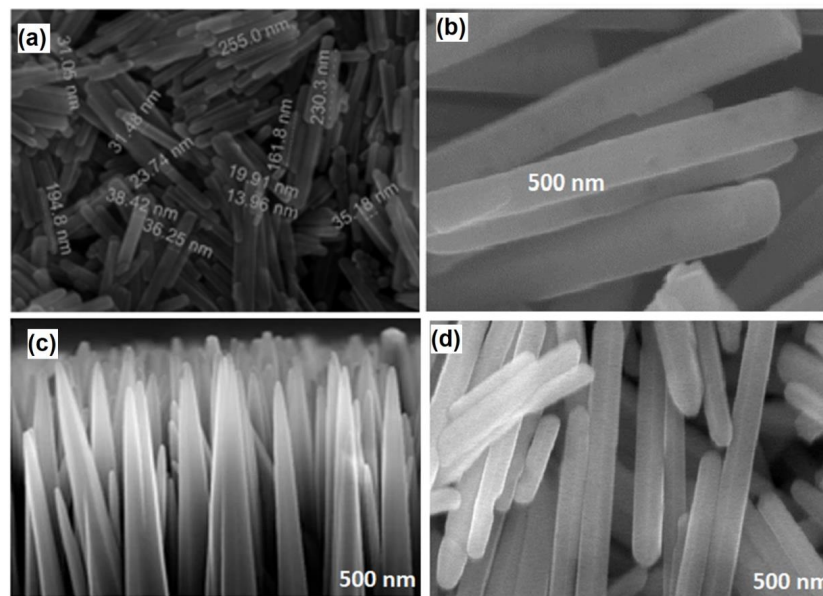


**Figure 5.** SEM images of ZnO nanorods obtained by varying (a) the growth time, (b) the reaction time, and (c) the lower hydrothermal temperature, (d) shows facile hydrothermal synthesis. Reproduced with permission from [54].

## 2.2. Sol–Gel Synthesis of ZnO nanostructures

The sol–gel method is considered the simplest and most well-established among the nanoparticle synthesis methods. It has the ability to control the size and morphology of the particles by systematic monitoring of the reaction parameters [45]. The principle of sol–gel synthesis is to ‘dissolve’ the compound (more accurately, disperse) in a liquid in order to redeploy it in a controlled manner. Multiaspect compounds can be organized with a managed stoichiometry by blending the sols of various compounds. The processing parameters (such as concentration, pH, the annealing temperature, additives such as surfactants) are systematically controlled during synthesis for the desired morphology, size, orientation, etc. [57]. These attributes affect the optical properties of the nanoparticles. The morphology can be regulated efficiently during sol–gel synthesis via hydrolysis and condensation reaction. The sol–gel technique avoids the issues of co-precipitation, which includes inhomogeneous and gelation reactions. It also encourages a more homogeneous blend at the atomic level and yields smaller particles without difficulty. This method occurs in 5 steps, hydrolysis, polycondensation, gelation, aging, drying, densification, and crystallization, as illustrated in Figure 6.

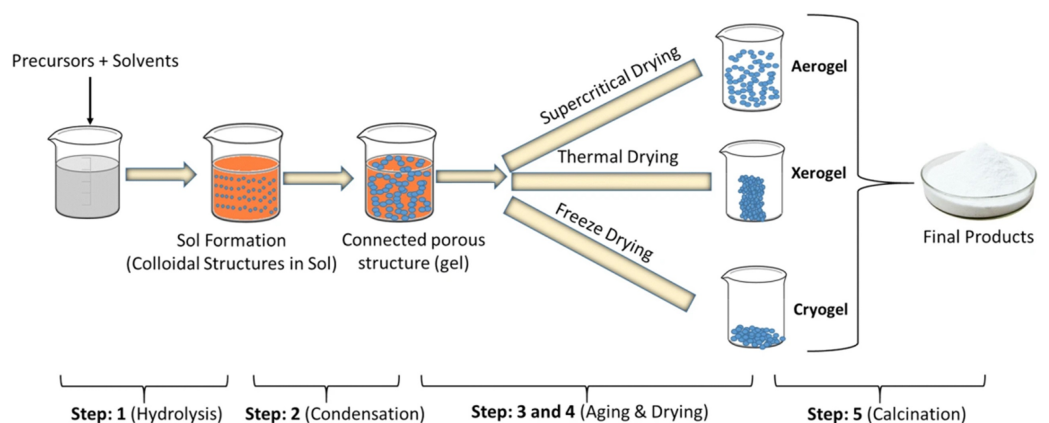


**Figure 6.** Schematic procedure of synthesizing nanomaterials via the sol–gel technique. Reproduced with permission from [57].



During hydrolysis, precursors such as metal alkoxides are dissolved in an aqueous or alcohol-based solvent (the “sol”) that provide an oxygen-rich medium that is beneficial for the formation of ZnO nanoparticles. The condensation stage of the process results in increased solvent viscosity, forming the “gel”. This is a porous structure that maintains a localized, semi-liquid phase. During the aging stage of the process, polycondensation continues within the localized solution along with precipitation of the gel network. This ultimately decreases porosity and increases the thickness of the colloidal particles. In the drying stage that follows, the solution is thermally treated, i.e., calcined to drive off the residues and water molecules from the sample, which is now predominantly ZnO nanoparticle-based. The calcination temperature is carefully controlled to achieve the desired pore size and material density. Khan et al [58] suggested that the mechanical speed of agitation and rotation in the synthesis protocol sol–gel method are important parameters that contribute to the size of the final ZnO nanoparticles. They showed that mechanical stirring during sol–gel synthesis forms thorn-like ZnO nanoparticles. In the literature, there are also several examples of the sol–gel method. For instance, flower petal-like ZnO nanoparticles spanning  $\sim 500$  nm at the top,  $\sim 1$   $\mu\text{m}$  at the bottom, and more than  $9$   $\mu\text{m}$  in length [55]. The particles were obtained using zinc nitrate  $\text{Zn}(\text{NO}_3)_2 \cdot 6\text{H}_2\text{O}$ , citric acid, and ethylene glycol as the source of  $\text{Zn}^{2+}$ , the chelating agent, and the solvent, respectively. In addition, a modified sol–gel method formed semispherical and flower-like ZnO nanoparticles [59]. They used zinc nitrate ( $\text{Zn}(\text{NO}_3)_2 \cdot 6\text{H}_2\text{O}$ ) as a  $\text{Zn}^{2+}$  source, triethanolamine ( $\text{C}_6\text{H}_{15}\text{O}_3\text{N}$ ), and citric acid ( $\text{C}_6\text{H}_8\text{O}_7$ ) as the chelating and gel agents, respectively. Figure 7 shows the SEM images of typical ZnO nanostructures using the sol–gel method.

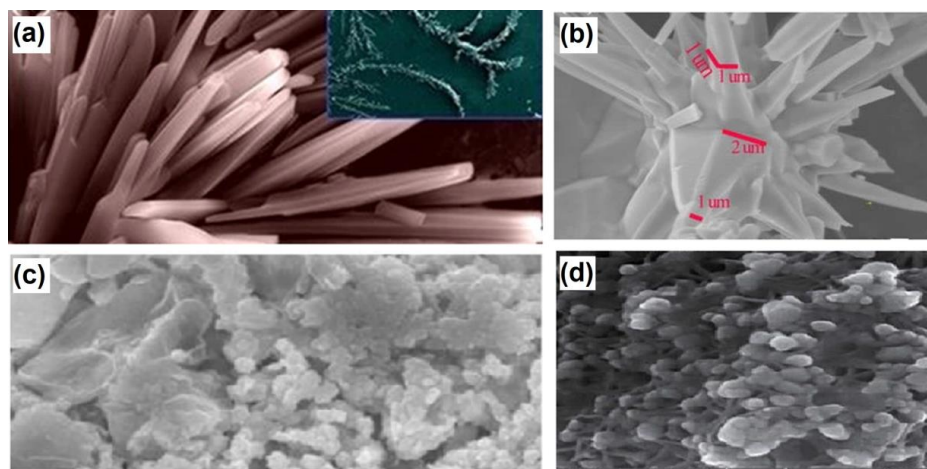


**Figure 7.** SEM images of different sol–gel synthesized ZnO nanostructures. (a) Thorn-like, (b) flower petals, (c) semispherical, and (d) spherical. Reproduced with permission from [56].

### 2.3. Chemical Bath Deposition Synthesis of ZnO Nanostructures

The chemical bath (or solution) deposition method has been used to synthesize a wide variety of metal oxide thin films on different substrates for a long time, although it is less popular than the sol–gel method. Only a vessel of an aqueous solution of a precursor can be reacted and precipitated in a controlled manner to form the desired metal oxide compound. It is essentially a two-step method that involves the formation of the solid phase from a precursor solution, nucleation, and particle growth. The method favors large-area thin films and is amenable to batch processing and continuous deposition. However, the formation of the thin film is highly sensitive to the pH of the chemical bath solution, bath temperature, deposition time, stirring rate, the concentration of the cations and anions, etc. Film growth occurs through ion condensation of material, or through the adsorption of colloidal material from the solution, on the substrate. The major benefits of this technique are its technical simplicity and excellent reproducibility. It yields a stable, uniform thin film

without physical substrate damage. Its major drawback is the abundant remnant solution making it considered wasteful and expensive. Figure 8 shows the facile and rapid chemical bath deposition setup and used by Strano et al. [60].

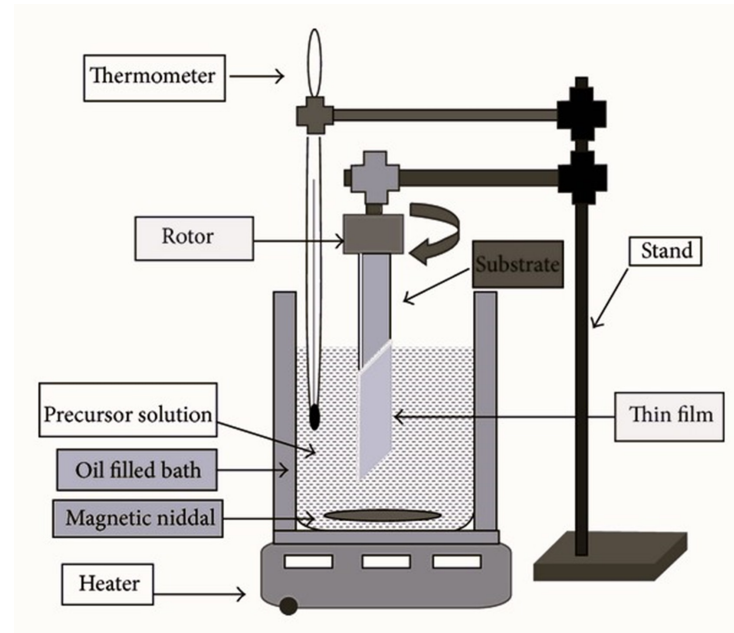


**Figure 8.** Overview of the setup for the chemical bath deposition method. Reproduced with permission from [60].

They managed to produce extended open-structured ZnO microflowers with a high reactive surface area. Figure 9 outlines the flow of the two-step method.

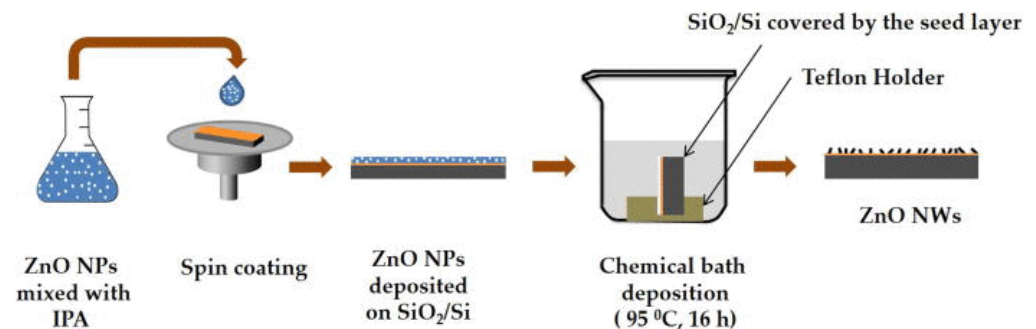


**Figure 9.** Schematic representation of the two-step method of the chemical bath deposition process. Reproduced with permission from [60].

The micro-flowers were composed of very thin sheets organized to form a spherical structure characterized by a large surface-to-volume ratio, which is also a key factor for improved charge transport in solar cells. The average diameters of the ZnO micro flowers were in the 0.2–2.5  $\mu\text{m}$  range. The formation was achieved by a complexing action of fluorine in an aqueous solution of zinc nitrate hexahydrate and hexamethylenetetramine. The growth catalyst or surfactant is now accepted to assist the tuning of ZnO nanostructure 1D, 2D, and 3D morphologies. Figure 10 shows SEM images of some examples of ZnO nanoparticles achievable using CBD.

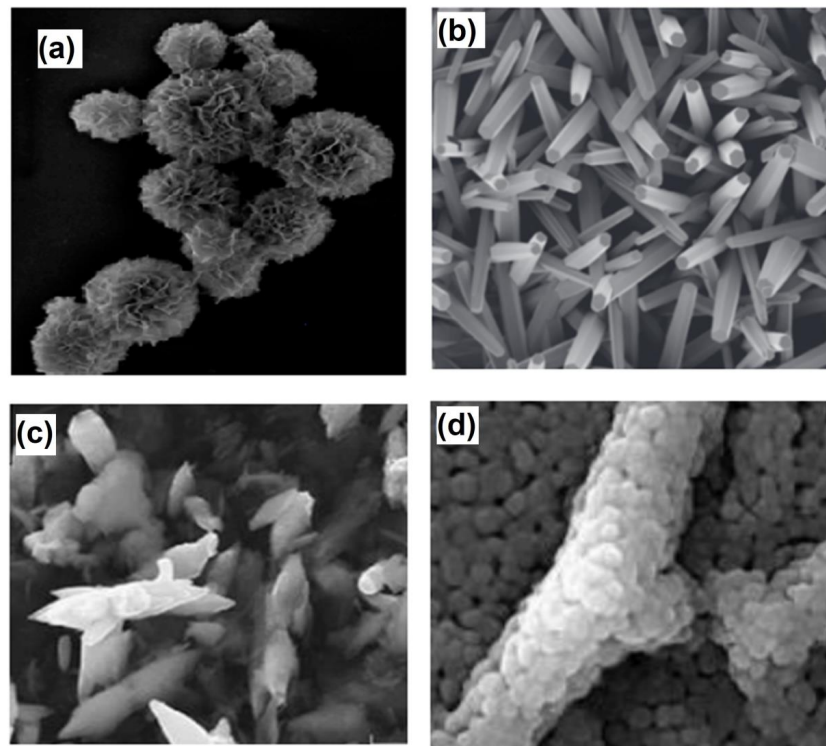


**Figure 10.** SEM images of ZnO nanoparticles achievable by varying CBD bath parameters. In (a) ZnO microflowers, in (b) ZnO nanorods, in (c) flake-like nanoparticles, and in (d) compact nanoparticle [61].

Mwankemwa et al. [61] examined the influence of ammonia solution as an external concentration control parameter on the growth of ZnO nanorods at low temperature (60 °C) CBD. The concentration of ammonia was seen to have an impact on the degree of supersaturation in the growth solution, causing a significant deviation in the morphology and crystal orientation of the ZnO nanorods. Dense nanorod arrays with diameters ranging from 60 to 90 nm were obtained. Similarly, Koao et al. [62] evaluated the effect of the pH bath varying different volumes of ammonia under constant time and bath temperature. They observed a combination of ZnO flakes-like and flower-like structures. Among all of the parameters that affect the chemical bath deposition method, the properties of the seed layer appear to exert a significant influence on the morphological features of the final ZnO nanorods. Earlier studies suggested that by varying the seed layer sol concentration, the quality of ZnO nanoparticles can be improved by regulating the Van der Waals forces in the sol step [55].

#### 2.4. Physical Vapour Deposition Synthesis of ZnO Nanostructures

The physical vapor deposition method is a bottom-up approach, as previously defined. The materials are evaporated in a vacuum to avoid impurities. This occurs by vapor particles traveling toward the substrate (cold target), and as soon as the vapor particles reach the substrate, they become condensed into solids. Vapor particles can be deposited into the substrate by the resistive method or by the sputtering method. In the resistive method, heat is generated to evaporate the material by passing a current through a high-resistance coil that is connected to a power supply. Similarly, the sputtering method is also a bottom-up approach where the material is sputtered in a vacuum and moves towards the substrate where they are deposited and condensed back into a solid state. However, in the sputtering method, high energy electrons are produced by an electron gun onto the target material and then evaporated to the substrate where they are deposited and condensed into solid particles. Different catalyst sizes affect the morphology of the resulting particles, either 1D, 2D, or 3D. Therefore, to obtain a more effective morphology, one needs to optimize

the parameters such as dye adsorption, electron transport, and network configuration. Jimenez-Cadena et al. [63] investigated the synthesis of various ZnO nanostructures using a physical vapor deposition process on a glass-ITO substrate. They showed that by using gold nanoparticles as catalysts through a single-step process, nanowires (1D structures) and nanosheets (2D structures) were obtained. Using a modified two-step process, they obtained 3D nano-architectures by a physical vapor decomposition process by varying temperature, pressure, deposition time, and gas carrier flux. Figure 11 shows SEM images of their results.

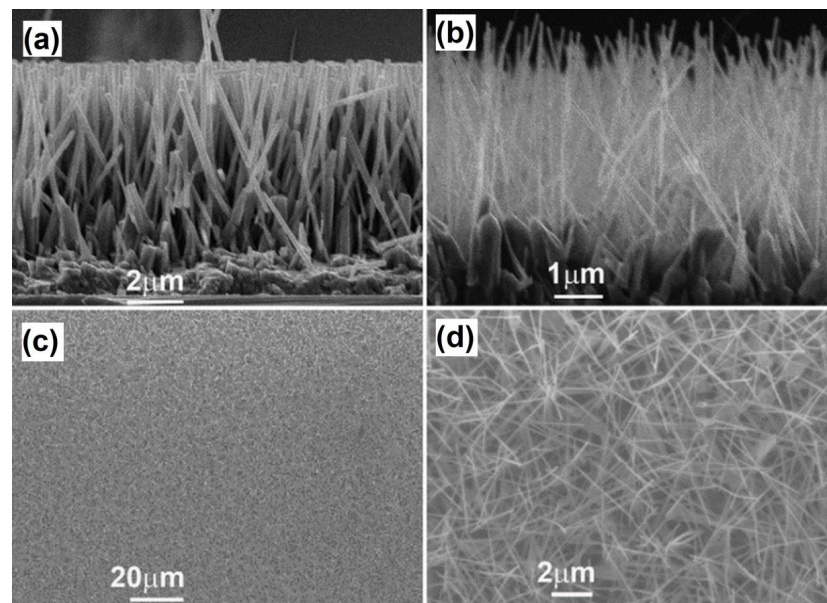


**Figure 11.** SEM images of the cross section of ZnO nanowire arrays at (a) 2  $\mu\text{m}$ , (b) 1  $\mu\text{m}$ , (c) 20  $\mu\text{m}$  and (d) the zoom-in view image of ZnO nanowires at 2  $\mu\text{m}$ . Reproduced with permission from [63].

Zhang et al. [64] also showed that using a physical vapor method that is free from a metal catalyst forms hexagonal well-faceted ZnO nanowire arrays at a temperature of 500  $^{\circ}\text{C}$ . These nanowire arrays are 1D, with an average diameter of 100 nm, and follow the c-axis direction of the wurtzite structure of ZnO. The ZnO nanowires and nanorods prepared by Barratto used physical vapor deposition by RF sputtering [65]. Xu et al. [66,67] established during the synthesis of ZnO nanowires from crystalline wurtzite by physical vapor deposition that the diameter and growth of ZnO nanoparticles increase as a function of growth temperature.

### 2.5. Plant Extract Synthesis of ZnO Nanostructures

Green synthesis methods were devised to limit the release of toxins into the environment. They are considered to be the safest approach for producing large-scales of large surface-area-to-volume ratio nanoparticles. Thus, they present a sharp contrast to the physical and chemical synthesis. One such method that can be considered green is the plant-extract method. It begins with washing and drying the plant (i.e., roots, leaves, stems, etc.) with distilled water at room temperature to remove any debris. The aerial parts of the plant are then finely ground into a powder, followed by the formation of an aqueous extract by cold maceration. This involves soaking the plant powder and then continuously agitating the suspension for some amount of time. The product is then filtered and stored at low temperature, as indicated in the schematic diagram in Figure 12.

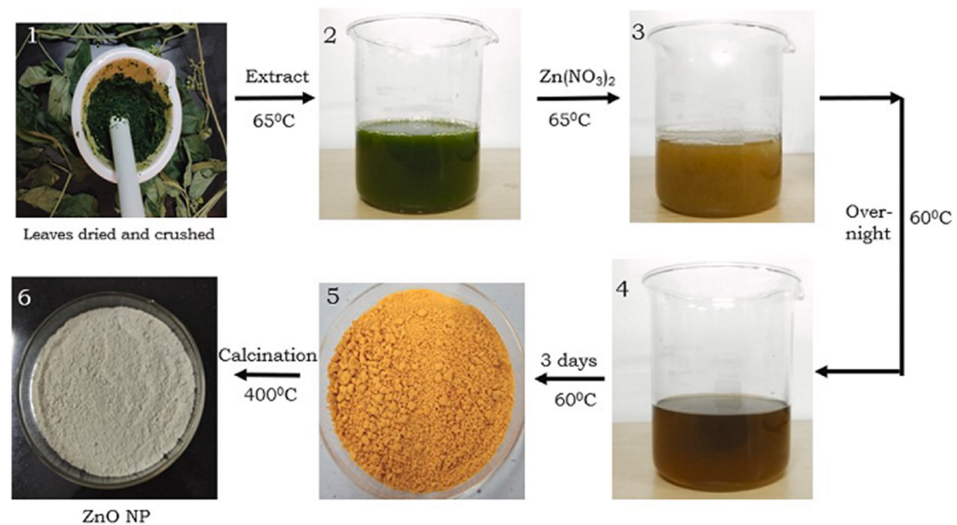


**Figure 12.** A schematic illustration of the plant extraction method. Reproduced with permission from [59].

Suresh et al. [68] used the extraction method on a plant called *artocarpus gomezianus* to synthesize ZnO nanoparticles. A hexagonal wurtzite structure with average crystallite sizes between approximately 5 and 15 nm was obtained. Similarly, Abdelkhalek et al. [69] extracted spherical ZnO nanoparticles with 74 nm sizes from the leaves of *mentha spicata*. Xu et al. [70] explored the factors that influence the morphology of ZnO NPs and their growth mechanism. The results indicated that the factors that influence morphology are preparation conditions, plant extract concentration, precursor concentration, reaction time, and calcination temperature [15,71–75]. The precursor concentration is the most significant factor affecting the morphology of ZnO nanoparticles. A pH of 12 was found to be appropriate for the synthesis of ZnO nanoparticles from plant extracts. Table 3 summarizes the synthesis routes, conditions, the resulting nanostructures, and the reported applications for the structures.

**Table 3.** A summary of the various ZnO synthesis methods, observed nanostructures, and reported applications.

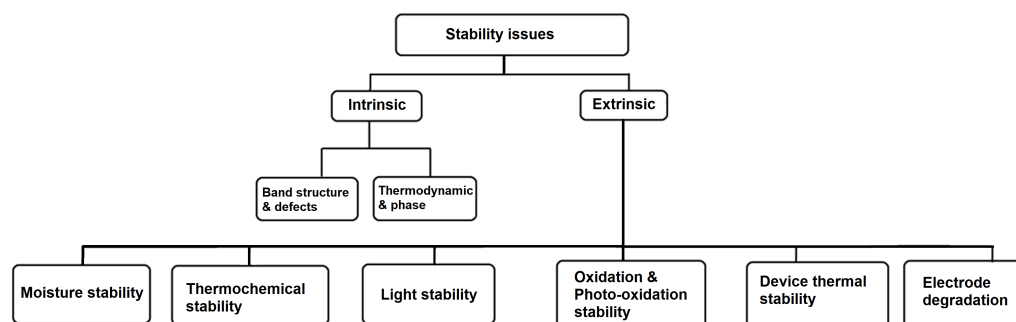
Method	Conditions	Nanostructure Attributes	Applications
Hydrothermal	Annealing at 90 °C for 180 min, growing for 10–15 h	Rice-shaped	ETL in DSSC [52]
	Reaction time: 3, 6, 9, 12 h	Tetrapods Nanorods (77–255 nm)	Photoanode in DSSC [53]
Hydrothermal (facile)	Low temperature (80 °C), short reaction time (2–10 h)	1D—vertically aligned nanorods	Gas sensing, solar cells [76]
Hydrothermal (2-step)	Growth at 90 °C and 100 °C, 6 h reaction time, Zinc acetate at 24 mM and 50 mM	Nanorods	Enhancing of electrical properties of MAPBI/ZnO/NR solar cells [48]
Hydrothermal	Low temperature	Good crystalline, 1D pencil-like nanorods	Sensors [10]
	150–450 °C	Long ZnO nanowire arrays	Enhancing of DSSC PCE [3]
Hydrothermal (One-pot)	Autoclaving at 140 °C for 12 h, Drying at 60 °C for 4 h	Nanowires (20–100 nm) diameter Nanobelts (80–250 nm) width	Sensors [76]

Table 3. Cont.

Method	Conditions	Nanostructure Attributes	Applications
Hydrothermal	Grown at 200 °C for 3 h	Highly crystalline wurtzite nanoflowers of (234–347 nm) length, (77–106 nm) diameter, 3.23 eV bandgap	Gas sensing, photodiodes, photodetectors, solar cells [57]
Hydrothermal (template-free)	Reactants as-is, 5 min grounding, autoclaved at 180 °C for 24 h and cooled to room temperature	Nanotubes (200–500 nm) length, (20–30 nm) diameter	Sensors [58]
Sol-gel	Incubation at 37 °C for 24 h	Thorn-like nanoparticles	Biological e.g., sunscreens [56]
	50 °C for 1 h, pH not controlled, drying at 250 °C for 1 h, heat-treated in air at 600 °C	Flower petal-like nanoparticles (500 nm at top, ~1 µm at bottom, and more than 9 µm length)	Optoelectronics [77]
Sol-gel (modified)	Stirred at 80 °C for 1 h, calcined at 120 °C for 1 h	Hexagonal wurtzite flower- and semi-spherical nanoparticles	Optoelectronics, removal of pollution [59]
PVD (2-step)	500 °C	1D nanowires, 2D nanosheets	DSSC [78]
PVD		Single crystal hexagonal wurtzite nanowires of ~100 nm diameter	Sensors [70]
CBD	Thermostatic bath control to 90 °C Growing at 60 °C Isothermal and isochoric conditions	Microflowers (0.2–2.5 µm) Nanorods (60–90 nm) diameter Nanoflakes and nanoflowers	Optoelectronics [63]
Plant Extract	Aqueous cassia fistula as fuel, preheated to 400 ± 10 °C, 5 min time Grown at 60 °C for 2 h, and dried at 60 °C overnight	Hexagonal wurtzite nanoparticles Spherical ZnO nanoparticles (74 nm) diameter	Biological [68,70]

### 3. Challenges and Future Directions of ZnO-Based PSCs

In this review, we have presented the state of the research and current questions concerning ZnO-based perovskite solar cells from the synthesis and fabrication of perovskite devices. To maintain focus, the present work has avoided classifying devices into inverted or noninverted types [79,80]. Recent progress in ZnO-based PSCs has improved the understanding of the impact of different 0D, 1D, 2D and 3D nanostructures and other synthesis conditions on overall device performance. This is evident in the upward trend in the PCE figure. When the first PSC devices were created, it was predicted that the performance of these devices would soon surpass that of silicon-based devices, not only in terms of PCE but also in terms of cost. However, despite significant progress, the primary issue of film-on-substrate stability remains the most pressing and recurrent theme. This poses a significant challenge for real-world application and commercialization. In ZnO-based devices, the vicinal surface and interfacial behaviors of heterogeneous layers are important. Recently, Shtepliuk et al. [81] showed a correlation between the structural and optical properties of these surfaces and interfaces in ZnO, using epitaxial films grown on SiC for nano-optoelectronic applications. Figure 13 is an overview of the main issues of device stability. These issues are broadly classified as either intrinsic, extrinsic or both.



**Figure 13.** A pictorial depiction of the stability issues in perovskite solar cells.

Intrinsic issues arise from the molecular and crystallographic structure of the perovskite material, while extrinsic issues are contingent on often unavoidable external factors. Such factors include, but are not limited to, encroaching moisture, oxygen, light, and thermal operating conditions. In photovoltaic applications, for example, the presence of moisture poses the most rapid degradation of the device [49]. In addition, device operating temperatures of 50 °C are expected in commercial solar cell modules, but can easily exceed 85 °C. Such conditions further compromise the integrity of the device. A visual cue is often presented by the device itself, where the nominally pristine black perovskite layer deposited on the ZnO layer yellows with temperature. Some concerted attempts are being made at the present time to improve stability. For instance, Ahmad et al. 2021 [82] employed ZnO and NiO<sub>x</sub> as the electron and hole transport layers, respectively. They reported that the device retained 83.82% of its original 8.97% PCE after 30 days in ambient air. They believed that the improved visible absorbance is due to the larger grain size and pin-hole filling in the CH<sub>3</sub>NH<sub>3</sub>PbI<sub>3</sub>-based photoactive layer. Another example of device stability and PCE improvement by doping was reported by Lin et al. [83], using SnO<sub>2</sub> doping of ZnO. They found a PCE of 20.45%. SnO<sub>2</sub> stacking on the ZnO layer improved interface contact by reducing the surface roughness and work function of the ITO layer and improved the electrical properties of the ETL. The overall result was an increase in crystallization in the perovskite. This improved the transport and extraction of charge at the interface. Recently, Rauwel et al. [84] found that the incorporation of Ag nanoparticles improved the absorption in ZnO-nanotubes by increasing the excitonic plasmon resonance and suppressing defect states. In summary, future research should focus on replacing lead with tin in a next-generation perovskite material. It should be noted that the toxicity of Pb is due to its reactivity. Such a strategy would also benefit the environment and be appealing for wider-scale production and deployment.

#### 4. Conclusions

This review provides detailed information on the effect of ZnO morphologies on perovskite solar cell performances and monitors the stepwise synthesis routes for obtaining the desired nano morphologies. The authors review previous studies and the latest developments in the synthesis methods, challenges, advantages, and contributions of controlling ZnO's ETM layer characteristics, particularly its shape, interfacial properties, trap states, and energy-level alignment, among the topics discussed. It is noted that the morphology and loading of the perovskite layer, the quality of the ZnO/perovskite interface, and the quality of the perovskite itself are all significantly impacted by variations in the nanostructures.

**Author Contributions:** Conceptualization, M.M., B.S.M., R.O.O., T.E.M. and T.D.M.; data collection, M.M., B.S.M., R.O.O., T.E.M. and T.D.M.; writing and editing, M.M., B.S.M., R.O.O., T.E.M. and T.D.M. All authors have read and agreed to the publication of the final version of the manuscript.

**Funding:** This research was funded by the National Research Foundation (NRF)/Thuthuka grant no. 137775.

**Institutional Review Board Statement:** This study did not involve any animal or human subjects.

**Informed Consent Statement:** Not applicable.

**Data Availability Statement:** No data included.

**Conflicts of Interest:** The authors declare no conflict of interest.

## References

1. Mahmood, K.; Swain, B.S.; Amassian, A. Double-layered ZnO nanostructures for efficient perovskite solar cells. *Nanoscale* **2014**, *6*, 14674–14678. [[CrossRef](#)] [[PubMed](#)]
2. Xu, F.; Dai, M.; Lu, Y.; Sun, L. Hierarchical ZnO nanowire- nanosheet architectures for high power conversion efficiency in dye-sensitized solar cells. *J. Phys. Chem. C* **2010**, *114*, 2776–2782. [[CrossRef](#)]
3. Feng, Y.; Ji, X.; Duan, J.; Zhu, J.; Jiang, J.; Ding, H.; Meng, G.; Ding, R.; Liu, J.; Hu, A.; et al. Synthesis of ZnO@ TiO<sub>2</sub> core-shell long nanowire arrays and their application on dye-sensitized solar cells. *J. Solid State Chem.* **2012**, *190*, 303–308. [[CrossRef](#)]
4. Djurišić, A.B.; Leung, Y.H. Optical properties of ZnO nanostructures. *Small* **2006**, *2*, 944–961. [[CrossRef](#)] [[PubMed](#)]
5. Pal, U.; Serrano, J.G.; Santiago, P.; Xiong, G.; Ucer, K.; Williams, R. Synthesis and optical properties of ZnO nanostructures with different morphologies. *Opt. Mater.* **2006**, *29*, 65–69. [[CrossRef](#)]
6. Fodjouong, G.J.; Feng, Y.; Sangare, M.; Huang, X. Synthesis of ZnO nanostructure films by thermal evaporation approach and their application in dye-sensitized solar cells. *Mater. Sci. Semicond. Process.* **2013**, *16*, 652–658. [[CrossRef](#)]
7. Li, D.; Haneda, H. Morphologies of zinc oxide particles and their effects on photocatalysis. *Chemosphere* **2003**, *51*, 129–137. [[CrossRef](#)]
8. Duan, J.; Xiong, Q.; Wang, H.; Zhang, J.; Hu, J. ZnO nanostructures for efficient perovskite solar cells. *J. Mater. Sci. Mater. Electron.* **2017**, *28*, 60–66. [[CrossRef](#)]
9. Galdámez-Martínez, A.; Santana, G.; Güell, F.; Martínez-Alanis, P.R.; Dutt, A. Photoluminescence of ZnO nanowires: A review. *Nanomaterials* **2020**, *10*, 857. [[CrossRef](#)]
10. Shouli, B.; Liangyuan, C.; Dianqing, L.; Wensheng, Y.; Pengcheng, Y.; Zhiyong, L.; Aifan, C.; Liu, C.C. Different morphologies of ZnO nanorods and their sensing property. *Sensors Actuators B Chem.* **2010**, *146*, 129–137. [[CrossRef](#)]
11. Fakharuddin, A.; Di Giacomo, F.; Ahmed, I.; Wali, Q.; Brown, T.M.; Jose, R. Role of morphology and crystallinity of electron transport layer on long term durable performance of perovskite solar cells. *J. Power Sources* **2015**, *283*, 61–67. [[CrossRef](#)]
12. Tang, J.F.; Tseng, Z.L.; Chen, L.C.; Chu, S.Y. ZnO nanowalls grown at low-temperature for electron collection in high-efficiency perovskite solar cells. *Sol. Energy Mater. Sol. Cells* **2016**, *154*, 18–22. [[CrossRef](#)]
13. Han, G.S.; Shim, H.W.; Lee, S.; Duff, M.L.; Lee, J.K. Low-Temperature Modification of ZnO Nanoparticles Film for Electron-Transport Layers in Perovskite Solar Cells. *ChemSusChem* **2017**, *10*, 2425–2430. [[CrossRef](#)]
14. Leonardi, S.G. Two-dimensional zinc oxide nanostructures for gas sensor applications. *Chemosensors* **2017**, *5*, 17. [[CrossRef](#)]
15. Schutt, K.; Nayak, P.K.; Ramadan, A.J.; Wenger, B.; Lin, Y.H.; Snaith, H.J. Overcoming zinc oxide interface instability with a methylammonium-free perovskite for high-performance solar cells. *Adv. Funct. Mater.* **2019**, *29*, 1900466. [[CrossRef](#)]
16. Mohamed Saheed, M.S.; Mohamed, N.M.; Singh, B.S.M.; Saheed, M.S.M.; Jose, R. Optoelectronic Enhancement of Perovskite Solar Cells through the Incorporation of Plasmonic Particles. *Micromachines* **2022**, *13*, 999. [[CrossRef](#)]
17. Pitchaiya, S.; Eswaramoorthy, N.; Natarajan, M.; Santhanam, A.; Ramakrishnan, V.M.; Asokan, V.; Palanichamy, P.; Palanisamy, B.; Kalimuthu, A.; Velauthapillai, D. Interfacing green synthesized flake like-ZnO with TiO<sub>2</sub> for bilayer electron extraction in perovskite solar cells. *New J. Chem.* **2020**, *44*, 8422–8433. [[CrossRef](#)]
18. Luo, J.; Wang, Y.; Zhang, Q. Progress in perovskite solar cells based on ZnO nanostructures. *Solar Energy* **2018**, *163*, 289–306. [[CrossRef](#)]
19. Li, S.; Zhang, P.; Chen, H.; Wang, Y.; Liu, D.; Wu, J.; Sarvari, H.; Chen, Z.D. Mesoporous PbI<sub>2</sub> assisted growth of large perovskite grains for efficient perovskite solar cells based on ZnO nanorods. *J. Power Sources* **2017**, *342*, 990–997. [[CrossRef](#)]
20. Eswaramoorthy, N.; Kamatchi, R. Planar perovskite solar cells: Eco-friendly synthesized cone-like ZnO nanostructure for efficient interfacial electron transport layer. *J. Mater. Sci. Mater. Electron.* **2021**, *32*, 24138–24151. [[CrossRef](#)]
21. Zeng, J.; Qi, Y.; Liu, Y.; Chen, D.; Ye, Z.; Jin, Y. ZnO-Based Electron-Transporting Layers for Perovskite Light-Emitting Diodes: Controlling the Interfacial Reactions. *J. Phys. Chem. Lett.* **2022**, *13*, 694–703. [[CrossRef](#)] [[PubMed](#)]
22. Yang, G.; Tao, H.; Qin, P.; Ke, W.; Fang, G. Recent progress in electron transport layers for efficient perovskite solar cells. *J. Mater. Chem. A* **2016**, *4*, 3970–3990. [[CrossRef](#)]
23. Zhou, H.; Yang, L.; Gui, P.; Grice, C.R.; Song, Z.; Wang, H.; Fang, G. Ga-doped ZnO nanorod scaffold for high-performance, hole-transport-layer-free, self-powered CH<sub>3</sub>NH<sub>3</sub>PbI<sub>3</sub> perovskite photodetectors. *Sol. Energy Mater. Sol. Cells* **2019**, *193*, 246–252. [[CrossRef](#)]
24. Kojima, A.; Teshima, K.; Shirai, Y.; Miyasaka, T. Organometal halide perovskites as visible-light sensitizers for photovoltaic cells. *J. Am. Chem. Soc.* **2009**, *131*, 6050–6051. [[CrossRef](#)]
25. Luo, L.; Lv, G.; Li, B.; Hu, X.; Jin, L.; Wang, J.; Tang, Y. Formation of aligned ZnO nanotube arrays by chemical etching and coupling with CdSe for photovoltaic application. *Thin Solid Films* **2010**, *518*, 5146–5152. [[CrossRef](#)]



26. Zhao, J.; Zheng, X.; Deng, Y.; Li, T.; Shao, Y.; Gruverman, A.; Shield, J.; Huang, J. Is Cu a stable electrode material in hybrid perovskite solar cells for a 30-year lifetime? *Energy Environ. Sci.* **2016**, *9*, 3650–3656. [[CrossRef](#)]
27. Dong, J.; Shi, J.; Li, D.; Luo, Y.; Meng, Q. Controlling the conduction band offset for highly efficient ZnO nanorods based perovskite solar cell. *Appl. Phys. Lett.* **2015**, *107*, 073507. [[CrossRef](#)]
28. Khan, F.; Kim, J.H. Enhanced charge-transportation properties of low-temperature processed Al-doped ZnO and its impact on PV cell parameters of organic-inorganic perovskite solar cells. *Solid-State Electron.* **2020**, *164*, 107714. [[CrossRef](#)]
29. Nagarjuna, Y.; Hsiao, Y.J. Au doping ZnO nanosheets sensing properties of ethanol gas prepared on MEMS device. *Coatings* **2020**, *10*, 945. [[CrossRef](#)]
30. Kumar, M.H.; Yantara, N.; Dharani, S.; Graetzel, M.; Mhaisalkar, S.; Boix, P.P.; Mathews, N. Flexible, low-temperature, solution processed ZnO-based perovskite solid state solar cells. *Chem. Commun.* **2013**, *49*, 11089–11091. [[CrossRef](#)]
31. Bi, D.; Boschloo, G.; Schwarzmüller, S.; Yang, L.; Johansson, E.M.; Hagfeldt, A. Efficient and stable CH<sub>3</sub>NH<sub>3</sub>PbI<sub>3</sub>-sensitized ZnO nanorod array solid-state solar cells. *Nanoscale* **2013**, *5*, 11686–11691. [[CrossRef](#)]
32. Zuo, L.; Gu, Z.; Ye, T.; Fu, W.; Wu, G.; Li, H.; Chen, H. Enhanced photovoltaic performance of CH<sub>3</sub>NH<sub>3</sub>PbI<sub>3</sub> perovskite solar cells through interfacial engineering using self-assembling monolayer. *J. Am. Chem. Soc.* **2015**, *137*, 2674–2679. [[CrossRef](#)]
33. Zhuiykov, S. *Nanostructured Semiconductor Oxides for the Next Generation of Electronics and Functional Devices: Properties and Applications*; Woodhead Publishing: Sawston, UK, 2014.
34. Xu, Y.; Liu, T.; Li, Z.; Feng, B.; Li, S.; Duan, J.; Ye, C.; Zhang, J.; Wang, H. Preparation and photovoltaic properties of perovskite solar cell based on ZnO nanorod arrays. *Appl. Surf. Sci.* **2016**, *388*, 89–96. [[CrossRef](#)]
35. Son, D.Y.; Im, J.H.; Kim, H.S.; Park, N.G. 11% efficient perovskite solar cell based on ZnO nanorods: An effective charge collection system. *J. Phys. Chem. C* **2014**, *118*, 16567–16573. [[CrossRef](#)]
36. Dong, J.; Zhao, Y.; Shi, J.; Wei, H.; Xiao, J.; Xu, X.; Luo, J.; Xu, J.; Li, D.; Luo, Y.; et al. Impressive enhancement in the cell performance of ZnO nanorod-based perovskite solar cells with Al-doped ZnO interfacial modification. *Chem. Commun.* **2014**, *50*, 13381–13384. [[CrossRef](#)]
37. Zheng, Y.; Zhao, E.; Meng, F.; Lai, X.; Dong, X.; Wu, J.; Tao, X. Iodine-doped ZnO nanopillar arrays for perovskite solar cells with high efficiency up to 18.24%. *J. Mater. Chem.* **2017**, *5*, 12416–12425. [[CrossRef](#)]
38. Wibowo, A.; Marsudi, M.A.; Amal, M.I.; Ananda, M.B.; Stephanie, R.; Ardy, H.; Diguna, L.J. ZnO nanostructured materials for emerging solar cell applications. *RSC Adv.* **2020**, *10*, 42838–42859. [[CrossRef](#)]
39. Dehghan, M.; Behjat, A. Deposition of zinc oxide as an electron transport layer in planar perovskite solar cells by spray and SILAR methods comparable with spin coating. *RSC Adv.* **2019**, *9*, 20917–20924. [[CrossRef](#)]
40. Zhang, R.; Fei, C.; Li, B.; Fu, H.; Tian, J.; Cao, G. Continuous size tuning of monodispersed ZnO nanoparticles and its size effect on the performance of perovskite solar cells. *ACS Appl. Mater. Interfaces* **2017**, *9*, 9785–9794. [[CrossRef](#)]
41. Iravani, S.; Korbekandi, H.; Mirmohammadi, S.V.; Zolfaghari, B. Synthesis of silver nanoparticles: Chemical, physical and biological methods. *Res. Pharm. Sci.* **2014**, *9*, 385.
42. Natsuki, J.; Natsuki, T.; Hashimoto, Y. A review of silver nanoparticles: Synthesis methods, properties and applications. *Int. J. Mater. Sci. Appl.* **2015**, *4*, 325–332. [[CrossRef](#)]
43. Gudikandula, K.; Charya Maringanti, S. Synthesis of silver nanoparticles by chemical and biological methods and their antimicrobial properties. *J. Exp. Nanosci.* **2016**, *11*, 714–721. [[CrossRef](#)]
44. Hasan, S. A review on nanoparticles: Their synthesis and types. *Res. J. Recent Sci.* **2015**, *2277*, 2502.
45. Nikam, A.; Prasad, B.; Kulkarni, A. Wet chemical synthesis of metal oxide nanoparticles: A review. *CrystEngComm* **2018**, *20*, 5091–5107. [[CrossRef](#)]
46. Yang, G.; Park, S.J. Conventional and microwave hydrothermal synthesis and application of functional materials: A review. *Materials* **2019**, *12*, 1177. [[CrossRef](#)]
47. Komarneni, S.; Roy, R.; Li, Q. Microwave-hydrothermal synthesis of ceramic powders. *Mater. Res. Bull.* **1992**, *27*, 1393–1405.
48. Solomon, G.; Mazzaro, R.; Morandi, V.; Concina, I.; Vomiero, A. Microwave-assisted vs. conventional hydrothermal synthesis of MoS<sub>2</sub> nanosheets: Application towards hydrogen evolution reaction. *Crystals* **2020**, *10*, 1040. [[CrossRef](#)]
49. Mahy, J.G.; Lejeune, L.; Haynes, T.; Body, N.; De Kreijger, S.; Elias, B.; Marcilli, R.H.M.; Fustin, C.A.; Hermans, S. Crystalline ZnO Photocatalysts Prepared at Ambient Temperature: Influence of Morphology on p-Nitrophenol Degradation in Water. *Catalysts* **2021**, *11*, 1182. [[CrossRef](#)]
50. Laila, I.K.; Mufti, N.; Maryam, S.; Fuad, A.; Taufiq, A.; Sunaryono. Synthesis and characterization of ZnO nanorods by hydrothermal methods and its application on perovskite solar cells. In Proceedings of the The 2017 International Conference on Mathematics, Science, and Education, Malang, East Java, Indonesia, 29–30 August 2017.
51. Noorasid, N.; Arith, F.; Alias, S.; Mustafa, A.; Roslan, H.; Johari, S.; Rahim, H.; Ismail, M. Synthesis of ZnO nanorod using hydrothermal technique for dye-sensitized solar cell application. In *Intelligent Manufacturing and Mechatronics*; Springer: Berlin, Germany, 2021; pp. 895–905.
52. Kumar, V.; Gupta, R.; Bansal, A. Hydrothermal Growth of ZnO Nanorods for Use in Dye-Sensitized Solar Cells. *ACS Appl. Nano Mater.* **2021**, *4*, 6212–6222. [[CrossRef](#)]
53. Nadargi, D.Y.; Tamboli, M.S.; Patil, S.S.; Mulla, I.S.; Suryavanshi, S.S. Development of Ag/ZnO nanorods and nanoplates at low hydrothermal temperature and time for acetone sensing application: An insight into spillover mechanism. *SN Appl. Sci.* **2019**, *1*, 1–10. [[CrossRef](#)]

54. Hu, H.; Huang, X.; Deng, C.; Chen, X.; Qian, Y. Hydrothermal synthesis of ZnO nanowires and nanobelts on a large scale. *Mater. Chem. Phys.* **2007**, *106*, 58–62. [[CrossRef](#)]
55. Wang, C.; Mao, B.; Wang, E.; Kang, Z.; Tian, C. Solution synthesis of ZnO nanotubes via a template-free hydrothermal route. *Solid State Commun.* **2007**, *141*, 620–623. [[CrossRef](#)]
56. Farhadi-Khouzani, M.; Fereshteh, Z.; Loghman-Estarki, M.R.; Razavi, R.S. Different morphologies of ZnO nanostructures via polymeric complex sol–gel method: Synthesis and characterization. *J. Sol–gel Sci. Technol.* **2012**, *64*, 193–199. [[CrossRef](#)]
57. Bokov, D.; Turki Jalil, A.; Chupradit, S.; Suksatan, W.; Javed Ansari, M.; Shewael, I.H.; Valiev, G.H.; Kianfar, E. Nanomaterial by sol–gel method: Synthesis and application. *Adv. Mater. Sci. Eng.* **2021**, *2021*, 5102014. [[CrossRef](#)]
58. Khan, H.; Habib, M.; Khan, A.; Boffito, D.C. A modified sol–gel synthesis to yield a stable Fe<sup>3+</sup>/ZnO photocatalyst: Degradation of water pollutants and mechanistic insights under UV and visible light. *J. Environ. Chem. Eng.* **2020**, *8*, 104282. [[CrossRef](#)]
59. Jayachandran, A.; Aswathy, T.; Nair, A.S. Green synthesis and characterization of zinc oxide nanoparticles using Cayratia pedata leaf extract. *Biochem. Biophys. Rep.* **2021**, *26*, 100995. [[CrossRef](#)]
60. Strano, V.; Greco, M.G.; Ciliberto, E.; Mirabella, S. ZnO Microflowers Grown by Chemical Bath Deposition: A Low-Cost Approach for Massive Production of Functional Nanostructures. *Chemosensors* **2019**, *7*, 62. [[CrossRef](#)]
61. Mwankemwa, B.S.; Nambala, F.J.; Kyeyune, F.; Hlatshwayo, T.T.; Nel, J.M.; Diale, M. Influence of ammonia concentration on the microstructure, electrical and raman properties of low temperature chemical bath deposited ZnO nanorods. *Mater. Sci. Semicond. Process.* **2017**, *71*, 209–216. [[CrossRef](#)]
62. Koao, L.; Dejene, F.; Swart, H. Effect of pH on the properties of ZnO nanostructures prepared by chemical bath deposition method. In Proceedings of the South African Institute of Physics 2015, Port Elizabeth, South Africa, 29 June–3 July 2015.
63. Jimenez-Cadena, G.; Comini, E.; Ferroni, M.; Vomiero, A.; Sberveglieri, G. Synthesis of different ZnO nanostructures by modified PVD process and potential use for dye-sensitized solar cells. *Mater. Chem. Phys.* **2010**, *124*, 694–698. [[CrossRef](#)]
64. Zhang, Y.; Jia, H.; Wang, R.; Chen, C.; Luo, X.; Yu, D.; Lee, C. Low-temperature growth and Raman scattering study of vertically aligned ZnO nanowires on Si substrate. *Appl. Phys. Lett.* **2003**, *83*, 4631–4633. [[CrossRef](#)]
65. Baratto, C. Growth and properties of ZnO nanorods by RF-sputtering for detection of toxic gases. *RSC Adv.* **2018**, *8*, 32038–32043. [[CrossRef](#)]
66. Xu, S.; Lao, C.; Weintraub, B.; Wang, Z.L. Density-controlled growth of aligned ZnO nanowire arrays by seedless chemical approach on smooth surfaces. *J. Mater. Res.* **2008**, *23*, 2072–2077. [[CrossRef](#)]
67. Xu, S.; Wei, Y.; Kirkham, M.; Liu, J.; Mai, W.; Davidovic, D.; Snyder, R.L.; Wang, Z.L. Patterned growth of vertically aligned ZnO nanowire arrays on inorganic substrates at low temperature without catalyst. *J. Am. Chem. Soc.* **2008**, *130*, 14958–14959. [[CrossRef](#)]
68. Suresh, S.; Pandikumar, A.; Murugesan, S.; Ramaraj, R.; Paul Raj, S. Metal-free low-cost organic dye-sensitized ZnO-nanorod photoanode for solid-state solar cell. *Mater. Express* **2011**, *1*, 307–314. [[CrossRef](#)]
69. Abdelkhalik, A.; Al-Askar, A.A. Green synthesized ZnO nanoparticles mediated by Mentha spicata extract induce plant systemic resistance against Tobacco mosaic virus. *Appl. Sci.* **2020**, *10*, 5054. [[CrossRef](#)]
70. Xu, J.; Huang, Y.; Zhu, S.; Abbes, N.; Jing, X.; Zhang, L. A review of the green synthesis of ZnO nanoparticles using plant extracts and their prospects for application in antibacterial textiles. *J. Eng. Fibers Fabr.* **2021**, *16*, 15589250211046242. [[CrossRef](#)]
71. Rakkesh, R.A.; Balakumar, S. Facile synthesis of ZnO/TiO<sub>2</sub> core–shell nanostructures and their photocatalytic activities. *J. Nanosci. Nanotechnol.* **2013**, *13*, 370–376. [[CrossRef](#)]
72. Lepot, N.; Van Bael, M.; Van den Rul, H.; D’Haen, J.; Peeters, R.; Franco, D.; Mullens, J. Synthesis of ZnO nanorods from aqueous solution. *Mater. Lett.* **2007**, *61*, 2624–2627. [[CrossRef](#)]
73. Tao, Y.; Fu, M.; Zhao, A.; He, D.; Wang, Y. The effect of seed layer on morphology of ZnO nanorod arrays grown by hydrothermal method. *J. Alloys Compd.* **2010**, *489*, 99–102. [[CrossRef](#)]
74. Hasnidawani, J.; Azlina, H.; Norita, H.; Bonnia, N.; Ratim, S.; Ali, E. Synthesis of ZnO nanostructures using sol–gel method. *Procedia Chem.* **2016**, *19*, 211–216. [[CrossRef](#)]
75. Arya, S.; Mahajan, P.; Mahajan, S.; Khosla, A.; Datt, R.; Gupta, V.; Young, S.J.; Oruganti, S.K. influence of processing parameters to control morphology and optical properties of Sol–gel synthesized ZnO nanoparticles. *ECS J. Solid State Sci. Technol.* **2021**, *10*, 023002. [[CrossRef](#)]
76. Ferreira, S.H.; Rovisco, A.S.; Santos, A.; Águas, H.; Igreja, R.; Barquinha, P.M.C.; Fortunato, E.; Martins, R. Porous ZnO nanostructures synthesized by microwave hydrothermal method for energy harvesting applications. *Nanopores* **2021**. [[CrossRef](#)]
77. Mousavi, S.F.; Davar, F.; Loghman-Estarki, M.R. Controllable synthesis of ZnO nanoflowers by the modified sol–gel method. *J. Mater. Sci. Mater.* **2016**, *27*, 12985–12995. [[CrossRef](#)]
78. Al-Asadi, A.S.; Henley, L.A.; Ghosh, S.; Quetz, A.; Dubenko, I.; Pradhan, N.; Balicas, L.; Perea-Lopez, N.; Carozo, V.; Lin, Z.; et al. Fabrication and characterization of ultraviolet photosensors from ZnO nanowires prepared using chemical bath deposition method. *J. Appl. Phys.* **2016**, *119*, 084306. [[CrossRef](#)]
79. Baltakesmez, A.; Biber, M.; Tüzemen, S. Inverted planar perovskite solar cells based on Al doped ZnO substrate. *J. Radiat. Res. Appl. Sci.* **2018**, *11*, 124–129. [[CrossRef](#)]
80. Zhang, F.; Xu, X.; Tang, W.; Zhang, J.; Zhuo, Z.; Wang, J.; Wang, J.; Xu, Z.; Wang, Y. Recent development of the inverted configuration organic solar cells. *Sol. Energy Mater. Sol. Cells* **2011**, *95*, 1785–1799. [[CrossRef](#)]

81. Shteplyuk, I.; Khranovskyy, V.; Ievtushenko, A.; Yakimova, R. Temperature-Dependent Photoluminescence of ZnO Thin Films Grown on Off-Axis SiC Substrates by APMOCVD. *Materials* **2021**, *14*, 1035. [[CrossRef](#)] [[PubMed](#)]
82. Ahmad, S.; Abbas, H.; Khan, M.B.; Nagal, V.; Hafiz, A.; Khan, Z.H. ZnO for stable and efficient perovskite bulk heterojunction solar cell fabricated under ambient atmosphere. *Solar Energy* **2021**, *216*, 164–170. [[CrossRef](#)]
83. Lin, L.; Yang, Z.; Jiang, E.; Wang, Z.; Yan, J.; Li, N.; Wang, Z.; Ai, Y.; Shou, C.; Yan, B.; et al. ZnO-modified anode for high-performance SnO<sub>2</sub>-based planar perovskite solar cells. *ACS Appl. Energy Mater.* **2019**, *2*, 7062–7069. [[CrossRef](#)]
84. Rauwel, P.; Galeckas, A.; Rauwel, E. Enhancing the UV emission in ZnO–cnt hybrid nanostructures via the surface plasmon resonance of Ag nanoparticles. *Nanomaterials* **2021**, *11*, 452. [[CrossRef](#)]